

# Registration for 3D Morphological Comparison of Brain Aneurysm Growth

Carl Lederman<sup>1</sup>, Luminita Vese<sup>1</sup> and Aichi Chien<sup>2\*</sup>

<sup>1</sup>Department of Mathematics, University of California, Los Angeles, Los Angeles, CA

<sup>2\*</sup>Division of Interventional Neuroradiology, Department of Radiological Sciences, University of California, Los Angeles, Los Angeles, CA [[aichi@ucla.edu](mailto:aichi@ucla.edu)]

**Abstract.** Recent advancements in 3D imaging technology have helped the early detection of brain aneurysms before aneurysm rupture. Developing management strategies for aneurysms has been an active research area. Because some unruptured aneurysms are followed up with medical images over years, there is immediate need for methods to quantitatively compare aneurysm morphology to study the growth. We present a novel registration method which utilized the volumetric elastic model specifically for this medical application. Validations to test the accuracy of the algorithm using phantom models were performed to determine the robustness of the method. Examples of the medical application using aneurysm images are shown and compared with their clinical presentation.

## 1 Introduction

Recent advancements in 3D imaging technology have helped the early detection of brain aneurysms before aneurysm rupture. Because of the high risks of mortality and morbidity related to aneurysm rupture, developing analysis strategies to evaluate the risk of rupture has been an active research area [1]. Many brain aneurysms are currently followed using medical images over years to monitor the growth without treatment. Recent studies have suggested that shape changes in these aneurysms may be an indication of increasing rupture risk and may need treatment to prevent rupture [2-3]. There is an immediate need for methods to analyze aneurysm growth, both for quantitative comparison of aneurysm geometry and to identify the location of growth to help treatment planning.

Image registration and morphometry generally refer to morphing one image until it resembles another image and analyzing the deformation that occurs during the morphing. This process can be used as a new approach to study the disease progression, especially for the type of disease which is related to geometrical changes of an organ or tissue, for example brain aneurysms. Related work for brain aneurysm registration was presented by Byrne et al., who registered a high quality 3D aneurysm image with a lower quality 2D image to assist surgical planning [4]. Craene et al. also presented a method to analyze the surgical outcome by comparing images of an aneurysm treatment coil at different time points using non-rigid registration [5]. Although medical applications for image registration have been well-developed, suitable algorithms to

study aneurysm growth are not available because the 3D registration of the entire aneurysm involves the registration of complex brain vessels around the aneurysm [6].

We present a new algorithm which can be applied to both aneurysms and complex vessel structure in the registration process. Our approach incorporates the elastic energy model in the registration and uses the surrounding blood vessels as the reference to orient the aneurysm and achieve alignment of the aneurysm (the round shape) and the blood vessel (the tubular shape).

## 2 Methods

### 2.1 Image Segmentation and Mesh Generation.

Standard clinical 3D angiographic images of brain aneurysms were used in this study. Images were acquired by digital subtraction angiography ( $0.34 \times 0.34 \times 0.34 \text{ mm}^3$ ) and computed topographic angiography ( $0.35 \times 0.35 \times 0.5 \text{ mm}^3$ ). The region-based binary segmentation method was applied to the 3D images with equal weights for the contrast region (blood vessel and aneurysm) and the background region [7]. The contrast region is assumed to be equal to 1 and the rest of the area is equal to 0 for the segmentation. (Fig. 1 (a) (b)) Based on the segmented 3D image, the tetrahedral mesh was generated for the entire blood vessel [8] (Fig. 1 (c)).

### 2.2 Volumetric Registration.

The registration process involves deforming a tetrahedral mesh by moving the nodes from an initial state  $X$  to a deformed state  $x$  [9]. We first define  $v = x - X$  so the registration is achieved by finding a  $v$  that minimizes an energy functional  $G$ .

$$G(v) = A(v) + E(v). \quad (1)$$

$G$  is the sum of two terms. The first is a data fidelity term using level sets,  $A$ , that deforms the mesh based on the geometry and the target image. The second term is a volumetric elastic energy  $E$ . By introducing an artificial time and morphing the mesh at each time step, we can reduce the energy function  $G$ . This formulation creates an interaction between the two terms ( $A(v)$  and  $E(v)$ ) during the morphing which does not occur in the registration method based on a fixed vector field [10].

Since a successful registration yields the morphed mesh which completely covers the target vessel, we define  $M$  (Equation (2)) to measure how well the mesh is morphed.

$$M = \frac{\int H(\phi_0(x - v(x)))I}{\int I} \in [0,1] \quad (2)$$

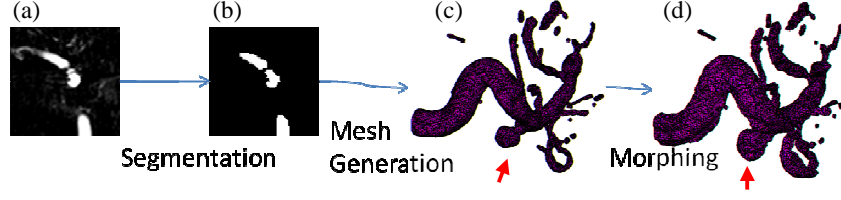


**Fig. 1.** The process of the proposed method including the segmentation, generation of triangular mesh, and registration using morphing (red arrows denote the aneurysm)

In Equation (2),  $H$  is the one dimensional Heaviside function, and  $I$  represents the target image.  $\varphi_0(x)$  is the distance to the boundary of the initial tetrahedral mesh generated from the initial image. If the two sets of images are perfectly matched,  $M$  is 1. Therefore, our proposed matching energy function  $A$  can be expressed as

$$A(v) = \int \delta(I-1)(1-H(\varphi_0(x-v(x)))) + M \int (1-\delta(I-1))H(\varphi_0(x-v(x))) \\ + (1-M) \int (1-\delta(I-1))(1-H(\varphi_0(x-v(x)))) \quad (3)$$

where  $\delta$  is the Dirac Delta function. A related model was proposed by Le Guyaler et al. [11] which introduced the nonlinear elastic smoother for a non-smooth 2D surface. In contrast, the energy  $A$  in our model includes the exact values of the Heaviside and Delta functions and is preferable for the problem—a smooth 2D boundary of a 3D object, the characteristics of blood vessel geometry.

Since minimizing  $A$  may result in large distortions, adding a regularization term  $E$  becomes important to provide a reasonable elastic response when large deformations occur. We implemented Mooney-Rivlin elasticity and calculated  $E$  directly on each tetrahedral element using the initial state,  $X$ , and final state  $x$ , by Equation (4) where  $F=d x/d X$  [12].

$$\nabla_x v = I - F^{-1} \quad (4)$$

The elasticity is defined in terms of rotationally invariant measures of the deformation using the Right Cauchy-Green deformation tensor  $C = F^T F$

$$J_1^C = \text{tr}(C), \quad J_2^C = \frac{1}{2}(\text{tr}(C)^2 - \text{tr}(C^2)), \quad J_3^C = \det(C) \quad (5)$$

The total elastic energy is achieved by taking an integral over all tetrahedral elements.

$$W = k_1 J_1^C + k_2 J_2^C + g(\sqrt{J_3^C}), \quad E(v) = \int W(\nabla v) \quad (6)$$

where  $g(x)$  is a quadratic function. The advantages of introducing the elastic energy include (1) helping to prevent undesirable large deformation due to drastic local shape changes and improve the morphing process. For example, when one part of the morphed mesh is in the correct location, it can pull nearby parts of the mesh into their correct locations based on elasticity. (2) as more of the morphed mesh matches the target region, the elastic energy can further improve the matching of the morphed mesh without changing  $A$ .

Although an easy way to reduce the total energy  $G$  at each time step is by implementing the standard gradient descent using the  $L^2$  inner product (Equation (7)), the standard gradient descent does not allow large time steps; therefore, longer computational time is needed for complicated vessel registration.

$$\frac{dv}{dt} = -\nabla_{L^2} G(v) \quad (7)$$

To speed up the computation for the clinical application, we applied the Sobolev gradient descent to reduce the total energy [13] (Equation (8)).

$$\frac{dv}{dt} = -\nabla_{H^1} G(v) = -(1 - K\Delta)^{-1} \nabla_{L^2} G(v) \quad (8)$$

where  $K$  is a positive constant and it only requires solving a linear system at each time step and allows for a much larger time step size than using the standard gradient descent.

### 3. Validations using Phantom Models

Synthetic data of phantom vessels were generated to test the robustness of the algorithm for the situation of vessel rotation and distortion. Because it is common to have slightly different head positions in clinical follow up images, we created an initial vessel (Fig 2 (a, left)) and target vessels with different rotation angles (Fig 2 (a, right)) to test how well the algorithm works in rotated images.

The follow-up images may be taken a few years after the initial images. Sometimes the vessel anatomy changes due to the disease and causes distortion of the angle between two connecting vessels. Therefore, it is important to know how well our approach can be applied to distorted vessel data. To test different degrees of distortion, we also created an initial vessel (Fig 3 (a, left)) and vessels with different distortion angles to define the target vessels (Fig 3 (a, right)).

Using the proposed registration algorithm, we were able to obtain the morphed vessels. Fig 2 (a, middle) and Fig 3 (a, middle) show the 2D slices of the morphed vessels for the tests of rotation and distortion, respectively.

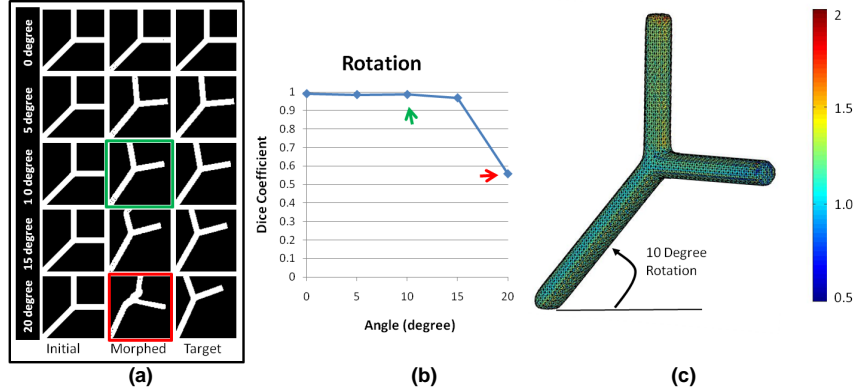


**Fig. 2.** Numerical experiments using synthetic vessel data with given rotation on the target image (a) shows the 2D slice of the initial, morphed, and target synthetic images. (b) shows the results of how the Dice coefficient changes for different rotation angles (c) is the representative results of the registration for the vessel rotated at 10 degrees. The colors are the triangle area of the morphed mesh element divided by area of the initial mesh element.

To compute how well the morphed vessel and target vessel match, the Dice coefficient was used to quantify the similarity [14]. The Dice coefficient is defined as

$$D(I, B) = \frac{2|I \cap B|}{|I| + |B|} \in [0, 1] \quad (9)$$

where  $I$  is the target vessel and  $B$  is the morphed vessel. The Dice coefficients for different degrees of rotation and distortion of the target vessels are shown in Fig 2 (b) and Fig 3 (b).

The matching results show that our method is adequate for the vessel geometry. It should be noted that although the target vessel which rotates 20 degrees from the original position is the limitation of the proposed method (Dice coefficient = 0.55, Fig 2 (a) red square, (b) red arrow), such rotation is beyond what can occur in brain aneurysm image data, because aneurysm images are acquired when the patient is lying down (face up) and the normal head rotation at that position is less than 10 degrees. Therefore, we found that for the application to analyze aneurysm growth, the proposed method can provide reliable results with high Dice coefficient.

We also examined the changes in triangle areas in the synthetic phantom vessels. Changes of triangle area can be the indication of aneurysm growth. Because in the phantom tests, there are only changes in angles and there are no changes in shape, we expected no area changes in the phantom vessel. Colors are used to represent the ratio of the triangle area of the morphed mesh to the triangle area of the initial mesh. Representative models are shown in Fig 2 (c) and Fig 3 (c). The uniform color on the vessels confirm that the algorithm correctly computed that there are no shape changes in the morphed vessels.

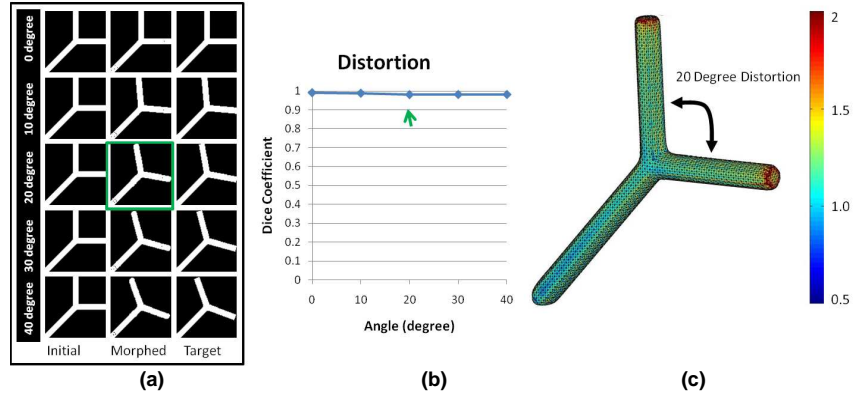


**Fig. 3.** Numerical experiments using synthetic vessel data with given distortion on vessel angles on the target. (a) shows the 2D slice of the initial, morphed, and target images. (b) shows the results of how the Dice coefficient changes for different distortion angles (c) is the representative results for vessel with 20 degree distortion (corresponds to the green indication in (a) and (b)). The colors are the area of the morphed mesh element divided by area in the initial mesh element.

#### 4. Registration of Clinical Aneurysm Images and Examinations of the Growth

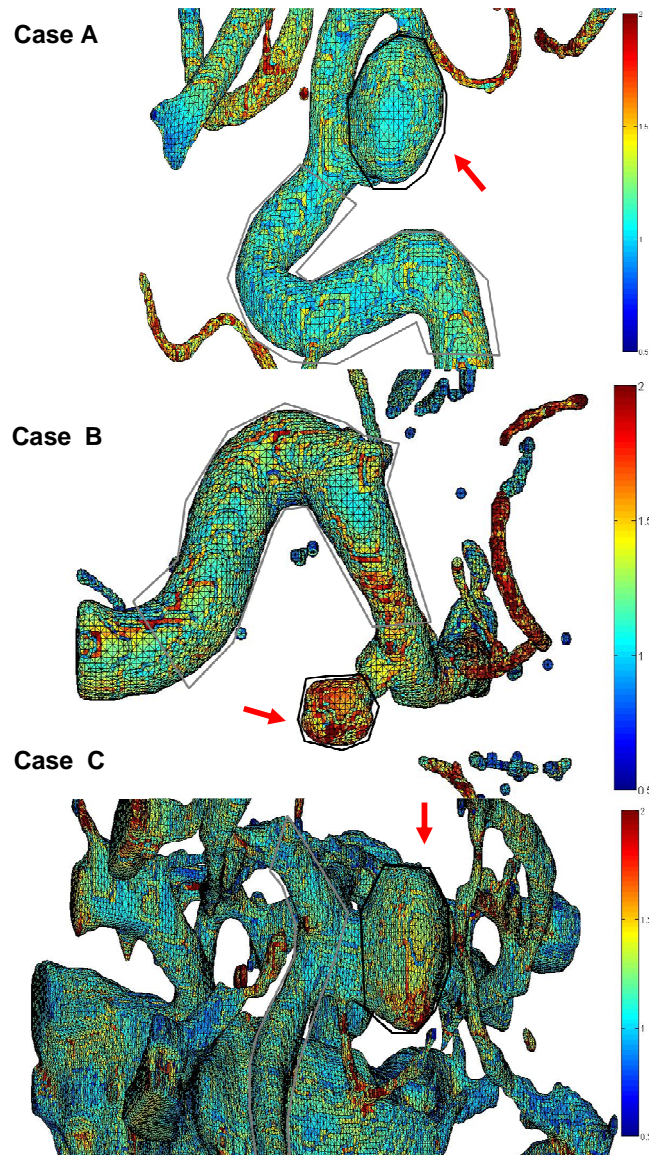
High resolution 3D images of brain aneurysm geometry acquired during patients' clinical examinations were analyzed using the proposed registration method. Each aneurysm has two sets of 3D images—an initial image and a follow-up image (target image). The morphed mesh is used to generate a visualization that shows changes in an aneurysm over time based on these two sets of images. The ratio of the triangle area of the morphed mesh to the triangle area of the initial mesh is denoted in color ranging from 0.5 (blue) to 2 (red). The higher ratio corresponds to increases in size.

Fig. 4 shows the result of registration for three aneurysms. The aneurysms are circled in black and denoted by red arrows. The large blood vessels are circled in gray. In case A, there is no overall difference in color in either the large blood vessel or aneurysm suggesting there is no growth at the aneurysm. This result is validated by the clinical report. In cases B and C, we observed clear changes in aneurysm size, denoted by the noticeably more red color of the aneurysms. This finding is in agreement with the clinical record. We also observed a wide range of deformation at areas with smaller blood vessels in all cases. This is due to the error generated during the segmentation process because those small vessels have diameter less than one or two voxels. These distortions, however, appear to have no effect on registration and morphing in the large blood vessel and aneurysm.

High resolution 3D images for brain vessels have become broadly used in clinical practice in recent years. There will be an increasing amount of aneurysm growth data to be collected and analyzed. We demonstrated the feasibility of the proposed method using three sets of clinical patient data. In the future, more patient data should be tested to further validate and improve the proposed algorithm.

#### **4 Conclusion**

We proposed a novel registration method to study aneurysm growth. This method matches 3D aneurysm images which were acquired at two different times from the same patient. We presented the validation study in phantom vessels and showed the medical application of this method. In all three presented patient cases, we were able to obtain and visualize the correct geometrical changes in the aneurysms which concurred with the clinical report. It is a feasible method for aneurysm growth analysis and provides valuable information and visualization for clinical aneurysm management.



**Fig. 4.** The colors give the triangle area in the morphed mesh divided by area in the initial mesh. The aneurysm is circled in black (indicated by red arrows) and the large blood vessel in grey. The aneurysm in case A shows no growth. Aneurysms in cases B and C show growth. The results concur with the clinical reports.

## References

- [1] Wiebers D.O., Whisnant J.P., Huston J., Meissner I., Brown R.D., Piepgras D.G., Forbes G.S. et al. Unruptured intracranial aneurysms: natural history, clinical outcome, and risks of surgical and endovascular treatment. *Lancet* 362(9378): 103-10 (2003).
- [2] Chien A, Sayre J, Vinuela F: Comparative Morphological Analysis of the Geometry of Rupture and Unruptured Aneurysms. *Neurosurgery* Mar 15 (2011).
- [3] Boussel L., Rayz V., McCulloch C., Martin A., Acevedo-Bolton G., Lawton M., Higashida R. et al.: Aneurysm growth occurs at region of low wall shear stress: patient-specific correlation of hemodynamics and growth in a longitudinal study. *Stroke* 39(11): 2997-3002 (2008).
- [4] Byrne J.V., Colominas C., Hipwell J., Cox T., Noble J.A., Penney G.P. Hawkes D.J.: Assessment of a technique for 2D–3D registration of cerebral intra-arterial angiography *The British Journal of Radiology*, 77, 123–128 (2004).
- [5] Craene, M., Pozo J., Cruz M., Vivas E., Sola T., Leopoldo G., Blasco J. et al : Coil Compaction and Aneurysm Growth: Image-based Quantification using Non-rigid Registration" *Medical Imaging 2008: Computer-Aided Diagnosis Proc. of SPIE Vol. 6915, 69151R, 1605-7422* (2008).
- [6] Thompson P.M., Giedd J., Woods R.P., MacDonald D., Evans A.C., Toga A.W.: Growth patterns in the developing brain detected by using continuum mechanical tensor maps. *Nature*, 404(6774) :190–3 (2000).
- [7] Chan T., Vese L.A.: Active Contours Without Edges. *IEEE Trans. Image Process.* 10(2), 266-277 (2001).
- [8] Lederman C., Joshi A., Dinov I., Vese L., Toga A., Van Horn J.: The generation of tetrahedral mesh models for neuroanatomical MRI, *NeuroImage* 55 (1): 153-164 (2011).
- [9] Hughes, T.: *The Finite Element Method: Linear Static and Dynamic Finite Element Analysis*, Englewood Cliffs, N.J.Prentice Hall, 109-182 (1987).
- [10] Christensen G.E., Rabbitt R.D., Miller M.I.: Deformable templates using large deformation kinematics. *IEEE Transactions on Image Processing*, 5(10):1435–1447 (1996)
- [11] Le Guyader C., Vese L.: A Combined Segmentation and Registration Framework with a nonlinear Elasticity Smoother. *UCLA C.A.M. Report 08-16* (2008).
- [12] Pedregal, P. *Variational Methods in Nonlinear Elasticity Society for Industrial and Applied Mathematics*, 1-6 (2000).
- [13] Neuberger, J. *Sobolev Gradients and Differential Equations*. Springer, 69-74 (1997)
- [14] Dice L.R.: Measures of the amount of ecologic association between species. *Ecology* 26:297–302 (1945).